Bioresource Technology Reports 24 (2023) 101640

Contents lists available at ScienceDirect

Bioresource Technology Reports

journal homepage: www.sciencedirect.com/journal/bioresource-technology-reports

Predictability and robustness of anode biofilm to changing potential in microbial electrolysis system

Melanie T. Knoll [1], Nikolai Jürgensen [1], Janek R. Weiler [1], Johannes Gescher [*]

Institute of Technical Microbiology, Hamburg University of Technology, Hamburg, Germany

ARTICLE INFO

Keywords:
Bioelectrochemical system
Microbial electrolysis cell
Rotating disc bioelectrochemical reactor
Electroactive biofilms
Biofilm robustness
Modeling of biological processes

ABSTRACT

Microbial electrolysis systems (MES) facilitate the process of using waste for efficient production of hydrogen thus resulting in lower energy costs compared to conventional hydrogen production. However, the stability and robustness of anode-respiring biofilms often limit long-term MES application. In this study, a 10 L rotating disc bioelectrochemical reactor was used to analyze the anodic biofilm under rapidly changing processing conditions, including changes in anode potential and shear force. A low complexity biofilm formed by *Shewanella oneidensis* and *Geobacter sulfurreducens* was studied to determine the boundary conditions for achievable current density and species interaction in large-scale applications. Demonstrating its robustness to the applied changes, the biofilm produced a stable current density of 1.2 A m^{-2} over 1.5 months. Furthermore, a mathematical model was developed to predict the behavior of the system in terms of current output, which may allow automatic user-defined control of sub-processes in MES reactors in the future.

1. Introduction

Bioelectrochemical systems (BES) facilitate the conversion of chemical into electrical energy using the interaction of exoelectrogenic microorganisms with solid state anodes. These organisms metabolize organic substrates and transfer the resulting respiratory electrons to the anode of a BES. The electrons are then either transferred to the cathode via an external resistor in microbial fuel cells (MFCs) to produce electricity or the electrons via an additional power supply are used to reduce protons to hydrogen in microbial electrolysis cells (MECs). To conduct efficient electron transfer, the organisms colonize the electrode surface in the form of a biofilm and utilize the anode as their terminal electron acceptor (TEA) to sustain their energy metabolism (Chaudhuri and Lovley, 2003; Logan, 2009). Thereby, the anode potential essentially controls the kinetics of electron transfer between the electrochemically active bacteria (EAB) and electrode and allows the process to direct the metabolism of the EABs that are colonizing the anode. At the same time, a lower anode potential will cause an increase in the energy gain per respiratory electron in an MFC system and will cause a decrease in the amount of energy needed to produce hydrogen in an MEC system. Hence, at least in the MEC, which typically offers more process control over the anode potential, interplay between anode potential, current density, hydrogen evolution rate, and necessary energy input exists.

The model organisms *Shewanella oneidensis* and *Geobacter sulfurreducens* are the most intensively studied anode-reducing organisms, and their synergistic effects in a mixed-species biofilm have been reported to exceed those of pure-culture biofilms of each organism (Dolch et al., 2014; Prokhorova et al., 2017; Engel et al., 2019). This difference may be in part due to the capability of *S. oneidensis* to metabolize various substrates to acetate, the preferred substrate of *G. sulfurreducens*, in addition to the capability of removing O_2 contamination that would negatively impact the productivity of *G. sulfurreducens*. The impact of lower applied anode potentials on the performance of this mixed-species model biofilm of *S. oneidensis* and *G. sulfurreducens* was previously reported in the study by Prokhorova et al. (2017). The authors first decreased and then increased the anode potential over nine days and demonstrated that the current production can not only be controlled but that the stability of the mixed-species biofilm was not negatively affected by the differences in achievable electron transfer rates to the electrode. Still, a long-term study of the stability and robustness of this mixed-species biofilm under rapidly changing conditions has not been conducted so far.

Several modeling approaches were developed to control and optimize BES (Recio-Garrido et al., 2016). Those models exist for MFC and

* Corresponding author.
E-mail address: johannes.gescher@tuhh.de (J. Gescher).
[1] All authors contributed equally to this work.

https://doi.org/10.1016/j.biteb.2023.101640
Received 20 July 2023; Received in revised form 21 September 2023; Accepted 24 September 2023
Available online 26 September 2023

MEC applications in different complexities that combine biological and electrochemical processes. Mathematical models were developed for calculations and predictions of the interaction between the microorganisms and the anode surface (Torres et al., 2007; Hamelers et al., 2011). In these studies, the Nernst–Monod (NM) model was introduced as a modification of the Monod model and used to describe the electrode as TEA mathematically. This model predicts the performance of the anode in terms of substrate dependency and the applied anode potential. Contrary to this model, the Butler–Volmer–Monod (BVM) model was developed as another analytical solution and describes the biochemical conversion and electron transfer reactions in a similar way as the NM model. These different approaches are useful for describing polarization curves (Torres et al., 2008; Hamelers et al., 2011) and the resulting parameters could be used for predictive simulation runs. Ultimately, these predictions form the basis for an automatic steering process based on varying parameters, including substrate availability and concentrations in addition to energy availability and price. These considerations would be particularly crucial for the application of BES in coupled processes, such as those proposed for MEC implementation in anaerobic digestion plants (Cerrillo et al., 2016; Yin et al., 2016; Hassanein et al., 2017), as these processes would allow user-defined, optimized operation of both sub-processes due to the controllability of the BES.

Several BES reactor systems have been introduced to study the efficiency of anodic biofilms (Kadier et al., 2016), but the scalability of these systems is often limited although an economically feasible scale-up would be a prerequisite for industrial applications. Recently, a novel rotating disc bioelectrochemical reactor (RDBER) was introduced (Hackbarth et al., 2023). This study introduced this scalable BES reactor system for the first time and provided insight into the general functionality and possible application of this reactor system as an MEC. In our study, a modified version of the RDBER was used to analyze the robustness of a model biofilm formed by the electroactive organisms *S. oneidensis* and *G. sulfurreducens* under various process conditions. With this low complexity community, this study aimed to analyze the boundary conditions for achievable current density and species interaction, respectively. Moreover, the interaction of the two organisms was previously described in small scale reactor systems (Prokhorova et al., 2017), and our intentions were to transfer this knowledge to larger scale. The predictability of the interaction was also chosen with the aim of developing a model with higher certainty. The experimental conditions were chosen to simulate operation parameters that are most likely to occur during the industrial application of BES. Thus, the applied potential and the rotational speed of the rotating anode discs were altered. The anode potential variation simulated a possible alternation in power supply during application, while a changing rotation was used to analyze the impact of shear force and diffusive mass transfer limitation of nutrients on the anodic biofilm catalyst. Further, a mathematical model was established to describe the current density as a function of these parameters and to enable future control of the RDBER's performance.

2. Materials and methods

2.1. Design and operation of 10 L rotating disc electrode reactor

A RDBER with a volume of 10 L was used as a three-electrode setup (Hackbarth et al., 2023). Graphite plates with a total area of 0.5 m^2 were used as an anode while titanium-coated half-discs with a total area of 0.2 m^2 were utilized as cathodes. In contrast to the procedure used by Hackbarth et al., the half-disc cathodes were mounted at the top of the corpus instead of the bottom. Metal tubes connected the 10 L reactor to a separate reference electrode chamber in which a SE23I reference electrode (Sensortechnik Meinsberg – Xylem, Waldheim, Germany) was setup (Fig. 1). Furthermore, the periphery included a mixing vessel with a pH probe. The pH was automatically adjusted by the fermenter control system Biostat® A (Sartorius AG, Göttingen, Germany). The RDBER and mixing vessels were temperature-controlled by installing custom-made silicon-heating mats (LCS Isotherm GmbH & Co. KG, Frankfurt, Germany) around the shell of the mixing vessel and the RDBER. All parts were connected by metal pipes with Ø 10 mm (Swagelok, Solon, Ohio,

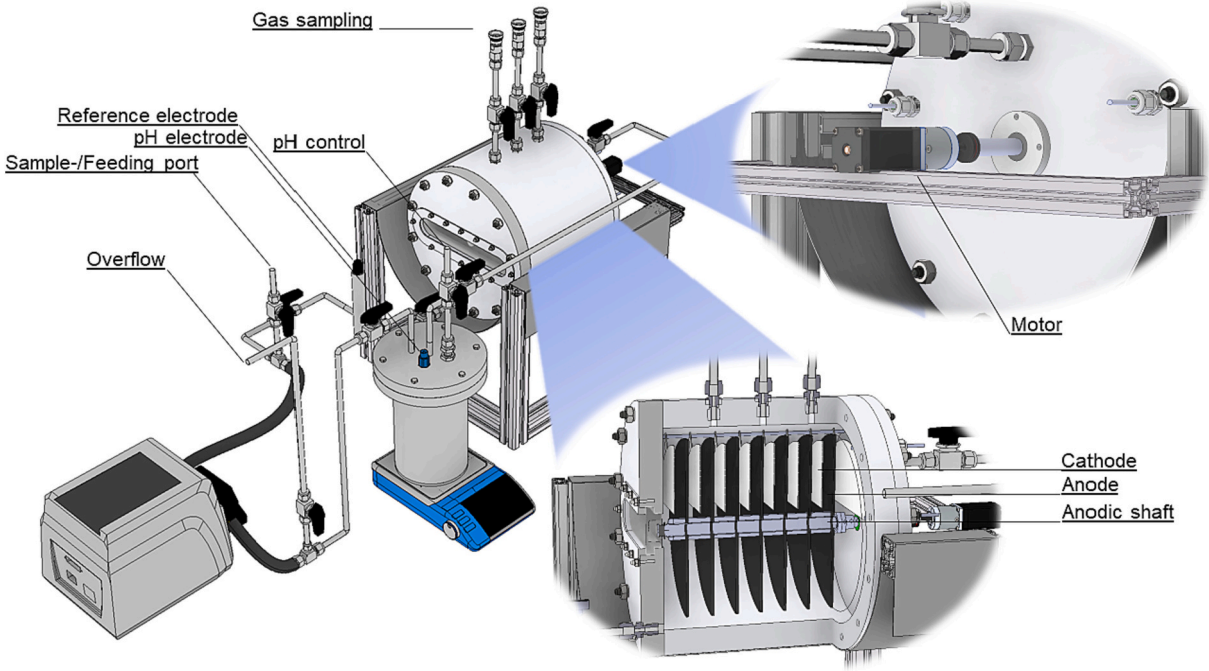

Fig. 1. Schematic of 10 L rotating disc bioelectrochemical reactor (RDBER) with periphery. The RDBER consisted of seven graphite plate electrode discs as working electrode (anode) with a total surface area of 0.5 m^2 and eight titanium coated half-discs as counter electrode (cathode) with a total surface area of 0.25 m^2. The surrounding periphery included a mixing vessel for pH control, ports for sampling and feeding, the reference electrode in addition to the tube pump, which was connected via gas-tight tubes to the metal pipes connected to the RDBER and the mixing vessel. A step motor was mounted to the anodic shaft for continuous control of the rotational speed of the anode discs.

US), except the pumping system. The tube pump (Masterflex™ L/S™ analog console pump with easy-load II pump heads Fisher Scientific, Schwerte, Germany) was connected to the metal pipes with gas-tight tubes (Masterflex™ L/S™ Viton™ FDA-compliant pump tubing, Fisher Scientific, Schwerte, Germany) to allow for a steering of the reactor using this peristaltic pump. The total volume of this reactor, including the periphery, was 12.6 L. For start-up, an additional tube was used to fill the reactor with the maximum volume of inoculated media described below. The anodic potential was kept at 0.199 V versus normalized hydrogen electrode (NHE) for the initial growth phase using a potentiostat (Interface 5000E, Gamry, Warminster, PA, USA); however, different anodic potentials and their influence on performance were studied. Here, the potentials were adjusted between −0.2 V and 0.2 V over different time intervals. The rotation of the anode discs inside the RDBER was kept at 1 RPM for the initial growth phase using a step motor (NEMA-11 bipolar stepper with 100:1 gearbox, Phidget, Calgary, Canada) that was mounted to the anodic shaft and ranged from 0.5 to 2 RPM when studying the influences of the changes in rotational speed. Current production, temperature, and pH were continuously logged. The measured current [A] was divided by the anode area [m^2] to calculate current density [A m^{-2}].

2.2. Growth conditions and strains

The operation of the RDBER was carried out with the wildtype strains *S. oneidensis* MR-1 (Venkateswaran et al., 1999) and *G. sulfurreducens* PCA (Caccavo et al., 1994). For the cultivation in the RDBER, a previously described anoxic medium containing 20 mmol L^{-1} lactate as electron donor was used (Knoll et al., 2022). To operate the reactor under fed-batch conditions, 20 mmol L^{-1} lactate was added every ~7.5 days. Furthermore, this medium contained several components per liter: (1) 1.8 g $NaHCO_3$, (2) 0.5 g Na_2CO_3, (3) 0.2 g $MgCl_2 \times 6$ H_2O, (4) 1.0 mL selenite-tungstate solution (0.5 g L^{-1} NaOH, 3.0 mg L^{-1} Na_2SeO_3, 4.0 mg L^{-1} Na_2WO_4), and (5) 100 mL salt solution (4.2 g L^{-1} KH_2PO_4, 2.2 g L^{-1} K_2HPO_4, 2.0 g L^{-1} NH_4Cl, 3.8 g L^{-1} KCl, 3.6 g L^{-1} NaCl). The medium was further complemented with 10.0 mL L^{-1} NB trace mineral solution (Coppi et al., 2001), 10.0 mL L^{-1} vitamin solution (German Type Culture Collection, DMSZ, media 141), 0.2 mmol L^{-1} sodium ascorbate, 0.4 mmol L^{-1} $CaCl_2$, and 0.1 % (*w/v*) yeast extract. The pH of the medium was adjusted to 7.0, and oxygen was removed by flushing with 80 % N_2/20 % CO_2. During operation of the RDBER, no flushing with N_2/CO_2 was done, and the system was not pressurized. *S. oneidensis* was pre-cultured at 30 °C in Luria Bertani (LB) media under oxic conditions over night while *G. sulfurreducens* was pre-cultivated at 30 °C for 48 h in the reactor media described above with 20 mmol L^{-1} acetate instead of lactate as electron donor and 20 mmol L^{-1} fumarate as electron acceptor. Before inoculation of the RDBER, the cells were harvested by centrifugation (10 min, 6000*g*) and washed twice with 1:10 diluted salt solution (see above). Thereafter, the cells were resuspended in 1:10 diluted salt solution. The optical density after inoculation was 0.1 with a 10:1 ratio of *S. oneidensis* ($OD_{600\ nm}$ = 0.09) and *G. sulfurreducens* ($OD_{600\ nm}$ = 0.01) cells. The RDBER was flushed with argon gas prior to the introduction of the inoculated medium to minimize oxygen contamination during the start-up of the system.

2.3. HPLC analysis

Organic acids were analyzed using a high-performance liquid chromatography (HPLC) analysis. A Dionex UltiMate 3000 HPLC (Thermo Scientific, Waltham, MA, US) with an Aminex HPX-87H column (Bio-Rad, Munich, Germany) and an integrated Refractive Index Detector RefractoMax520 (ERC, Riemerling, Germany) were used to quantify lactate consumption and acetate in addition to formate production. Samples were filtered with a 0.2 µm polyethyltetrafluoroethylene (PTFE) filter (VWR, Darmstadt, Germany), and 150 µL sample were added to 15 µL 0.5 mol L^{-1} sulfuric acid prior to analysis. Sulfuric acid (5 mmol L^{-1}) was used as an eluent, and the column temperature was set to 60 °C.

2.4. Calculation of coulombic efficiency

The coulombic efficiency (CE) indicates the ratio of measured current to the metabolically released electrons. To calculate this value, the total current was first determined by integrating the resulting current (I) in reference to the operation time (t) of 46 days. Furthermore, this current was divided by the total amount of metabolically released electrons. The latter was determined by the amount of lactate consumption (Δc), the reactor volume (V_R = 12.6 L), the number of electrons released from metabolizing 1 mol of lactate to CO_2 (z_e = 12), the elementary charge ($\epsilon = 1.602 \times 10^{-19}$C), and the Avogadro constant ($N_A = 6.022 \times 10^{23}$ mol^{-1}) as shown in Eq. (1).

$$CE = \frac{\int_{t_0}^{t} I\ dt}{\Delta c \cdot V_R \cdot z_e \cdot \epsilon \cdot N_A} \quad (1)$$

The total amount of lactate consumed during the 46 days of RDBER operation was calculated by subtracting the lactate concentration in the electrolyte at the end of operation from the total amount of lactate provided for the organisms during the 46 days of operation. Concentrations of organic acids were determined using HPLC as described above.

2.5. Calculation of shear force based on rotational speed of RDBER anodes

The rotational speed of the RDBER anodes was varied from 0.5 to 2 RPM in this study. These differences correspond to changes in the shear force that was applied to the biofilm. The shear force τ_w at the disc surface in a similar reactor system was calculated (Eq. (2)) as reported before (Möhle et al., 2007) depending on the radius of the discs (outer rim of the anode discs with $r = 0.105$ m), the density of the surrounding medium (aqueous medium with $\rho = 997$ kg m^{-3}), the rotational velocity (ω = rotational speed divided by 60), and the kinematic viscosity (aqueous medium with $\nu = 1 \times 10^{-6}$ m^2 s^{-1}).

$$\tau_w = 0.8 \cdot \rho \cdot \sqrt{\upsilon} \cdot \omega^{\frac{3}{2}} \cdot r \quad (2)$$

Thereby, the shear force that was applied to the anodic biofilm was altered from 6.4×10^{-5} N m^{-2} for 0.5 RPM to 1.8×10^{-4} N m^{-2} for 1 RPM and 5.1×10^{-4} N m^{-2} for 2 RPM.

2.6. Modeling of MEC reactor

2.6.1. Process model

A kinetic model was used to represent the experimental data derived from polarization curves and applied potential changes within the MEC. To describe the resulting current density of electrochemically active microorganisms on an anode, the BVM and NM models were chosen (Hamelers et al., 2011).

$$I = I_{max} \cdot \left(\frac{1 - e^{-\frac{F}{R \cdot T} \cdot \eta}}{K_1 \cdot e^{-(1-\alpha)\frac{F}{R \cdot T}\eta} + K_2 \cdot e^{-\frac{F}{R \cdot T}\eta} + 1} \right) \cdot \left(\frac{S}{\frac{K_M}{K_1 \cdot e^{-(1-\alpha)\frac{F}{R \cdot T}\eta} + K_2 \cdot e^{\frac{F}{R \cdot T}\eta} + 1} + S} \right) \quad (3)$$

The BVM (Eq. (3)) and NM models (Eq. (4)) consist of a term describing the potential dependency of the current density and the Monod term, which together defines the dependency of the substrate.

$$I = I_{max} \cdot \left(\frac{1}{1 + e^{-\frac{F}{R \cdot T}(E - E_{KA})}} \right) \cdot \left(\frac{S}{K_s + S} \right) \quad (4)$$

The calculation is a steady-state solution for the current density as a function of overpotential η defined as $E_A - E_{S/P}$ in which E_A is the anode

potential (V) and $E_{S/P}$ is the redox potential of acetate (V) (Hamelers et al., 2011). The transfer coefficient, α, has a value between 0 and 1, but for most electrochemical reactions, this coefficient is typically around 0.5 (Maurya et al., 2022). F is the Faraday constant (96,485C mol^{-1}), R the ideal gas constant (8.314 $J\ mol^{-1}\ K^{-1}$), and T the temperature (303 K). E represents the anode potential, and E_{KA} is defined as the potential for the half maximum rate at which $I = \frac{I_{max}}{2}$, that is −0.155 V versus the normal hydrogen electrode (NHE) as described by Torres et al. (2008).

K_M and K_S describe the substrate affinity of the substrate, S. The parameters K_1 and K_2 describe fundamental processes. K_1 describes the rate of the biochemical reaction compared to the electrochemical reaction (Hamelers et al., 2011). The parameter K_2 describes the ratio of the forward compared to the backward reaction of the redox component (Hamelers et al., 2011). The maximum resulting current density represents the parameter, I_{max}, and is a main limiting factor in addition to the anode potential for the calculation of the current density, I.

2.6.2. Parameter estimation

The individual model structure and related procedures for process simulation and parameter estimation were implemented in Matlab (The MathWorks, Inc., USA, Version 2020b). Parameters were determined by embedding the Levenberg-Marquardt and trust-region-reflective methods using the built-in solver "lsqnonlin" from Matlab. In that software system, parameter estimation was conducted to determine by sum of least squared error between measurements and corresponding simulation results values for the kinetic model. To evaluate the fitted parameters and the simulated data, the coefficient of determination R^2 (Eq. (5)) was calculated from the residual of 1 minus the ratio of the squared differences between the experimental data y_i and the simulated data y_s in addition to the squared differences between the experimental data and the mean value $\bar{y}$ (Arndt et al., 2021). The coefficient of determination is equal to 1 when the simulated data are in agreement with the measured experimental data (Moser et al., 2021).

$$R^2 = 1 - \frac{\sum_{i=1}^{n} (y_i - y_s)^2}{\sum_{i=1}^{n} (y_i - \bar{y})^2} \quad (5)$$

2.6.3. Monte Carlo-based uncertainty bands

To represent the uncertainty propagation and model parametric uncertainty of the process variability, uncertainty bands were determined. Therefore, 1000 simulations with a normally distributed standard deviation of 5 % were performed using the "prctile" function in Matlab to calculate the mean and the 10 % and 90 % quantiles of each model parameter distribution. Simulations of the linear sweep voltammetry were then performed using the mean and 10 % and 90 % quantile model parameter values.

3. Results

3.1. Operation of rotating disc bioelectrochemical reactor

To test the robustness and stability of a microbial electrolysis system, a 10 L RDBER was analyzed regarding its performance under various process conditions. The reactor was inoculated with *S. oneidensis* and *G. sulfurreducens* as test organisms, and after 12 days, a stable current density of 1.2 A m^{-2} was achieved at an anode potential of 0.199 V versus the NHE (Fig. 2). The RDBER reactor was operated for 46 days while various process conditions were applied. The maximum current density was found at day 14 with 1.8 A m^{-2}, while an average current density of 1.2 ± 0.2 A m^{-2} was achieved over the whole-time course of the experiment. To calculate the coulombic efficiency (CE) of the reactor system, the overall measured current was determined by integration. This calculation yielded a total value of 2,069,805C. Further, the metabolically released electrons were calculated based on the total lactate consumption. To this end, the final concentration of lactate on day 46 (14.8 mmol l^{-1}) was subtracted from the total amount of supplied lactate. The latter was based on the initial concentration of 20 mmol L^{-1} in the cultivation medium and the sum of six feeding events with 20 mmol L^{-1} each as described above, which resulted in a total lactate consumption of 125.2 mmol L^{-1}. Using the formula described above, a CE of 113.3 % was calculated for the RDBER system in this work. Notably, acetate or other carboxylic acids could not be detected during reactor operation suggesting efficient cross feeding between the two organisms.

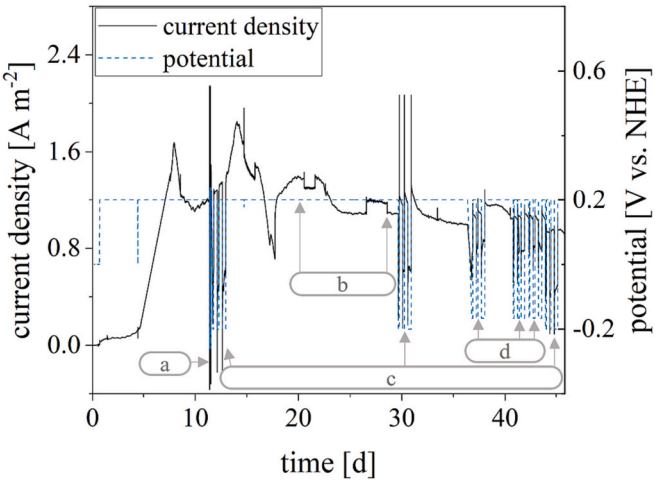

Fig. 2. Overview of 46 days of RDBER performance. Analyses were performed throughout the run including correlation of potential with current density using linear sweep voltammetry (a, Fig. 3), influences of changes in rotational speed of disc electrodes (b, Fig. 5) and influences of alternating applied potentials (c with 20 % and d with 50 % electron flux toward MEC, Fig. 4).

After the initial growth phase, a linear sweep voltammetry was performed, in which the applied potential was decreased from 0.24 V versus the NHE to −0.26 V in a step size of 0.25 mV s^{-1} and then increased using the same increment (Fig. 3). When decreasing the potential, a current density of 0 A m^{-2} was measured at a potential of −0.24 V. Consequently, in the following experiments, 0 A m^{-2} was determined as 0 % electron flux from the organisms to the anode at a potential of −0.24 V although we observed a minor deviation to a slightly more negative value when the linear sweep was conducted with increasing anode potentials.

3.2. Manipulating electron flux

Current density and the consequent electron flux of the system are directly linked to the applied potential. The robustness of the system was tested by intentionally manipulating the electron flux of the system to lower percentages. As a proof-of-principle, 20 % and 50 % electron fluxes were selected with respect to the stable average current density of 1.2 A m^{-2}. The corresponding potential of −0.2 V and −0.17 V for 20 % and 50 % electron flux, respectively, were then taken from the linear sweep data set (Fig. 3) and time periods of 2, 4, and 8 h were chosen. Each cycle was followed by an interval of 8 h of 100 % electron flux (Fig. 4). This regime of changing the anode potential was applied six times in total to yield replicate data. At 20 % electron flux, the average current density for 2, 4, and 8 h was measured to be 0.5 A m^{-2}, while 50 % electron flux resulted in an average current density of approximately 0.75 A m^{-2}. Interestingly, these resulting current densities were higher than the expected values of 0.24 and 0.6 A m^{-2} with respect to the linear sweep. When the electron flow was reduced from 100 % to 20 % or 50 %, it took approximately 1.5 h for the monitored current density to stabilize at the previously mentioned values of 0.5 or 0.75 A m^{-2}. However, when the electron flow was increased, stable current production was observed at 1.2 A m^{-2} without any adaptation time.

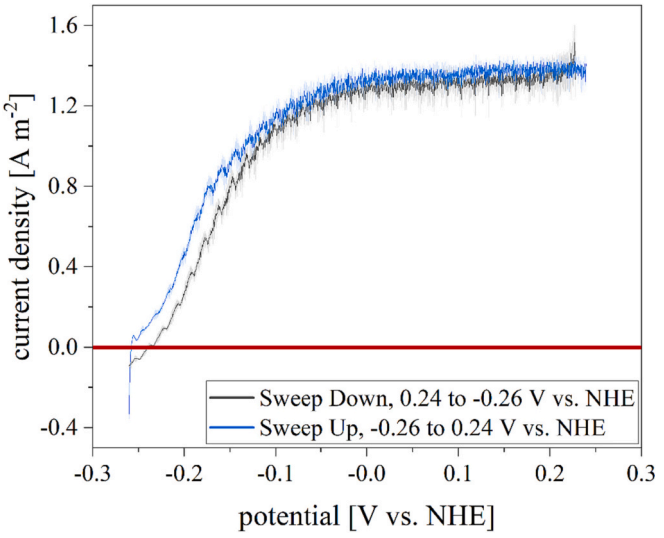

Fig. 3. Current density correlated with time and different potentials. After the initial growth phase (day 12), a linear sweep voltammetry was performed in triplicates. The potential was swept from 0.24 V to −0.26 V (sweep down) versus the normal hydrogen electrode (NHE) and vice versa (sweep up) with a sweep rate of 0.25 mV s^{-1}. The red line indicates the threshold of 0 A m^{-2} current density and the corresponding potential was −0.24 V for the sweep down and −0.258 V for the sweep up. This sweep was the basis for the potential alterations and the chosen potentials (Fig. 4). The robustness of the system was analyzed over 46 days and current density as a factor of stability was monitored. The current density stabilized around 1.2 A m^{-2}. (For interpretation of the references to colour in this figure legend, the reader is referred to the web version of this article.)

3.3. Influence of rotational speed on current density

The rotational speed of the rotating disc anodes was altered to analyze the potential impact of shear force and diffusive mass transfer on the process. The default rotational speed was set to 1 RPM that corresponded to a shear force of 1.8×10^{-4} N m^{-2}. This speed was then decreased to 0.5 RPM and a shear force of 6.4×10^{-5} N m^{-2} for one day followed by an interval of 1 RPM for approximately four days before the speed was increased to 2 RPM and a shear force of 5.1×10^{-4} N m^{-2} for approximately two days (Fig. 5). After a rotational speed of 0.5 RPM was applied, and the shear stress was reduced, current density declined from 1.38 A m^{-2} to 1.3 A m^{-2}. During the interval of 1 RPM, current density slowly decreased to a stable value of 1.1 A m^{-2}. The application of 2 RPM and increase in shear force led to an increase in current density to 1.2 A m^{-2}, whereas the same current density of 1.1 A m^{-2} was again measured as soon as 1 RPM was applied again.

3.4. Model for predictability and automatic steering of RDBER

Linear sweep voltammetry was performed after the initial growth phase by decreasing and increasing the applied potential with increment/decrements of 0.25 mV s^{-1}. The resulting curves were fitted with the BVM and NM models, including the 10 % and 90 % quantiles of the Monte Carlo-based simulation (Fig. 6).

Both models describe the experimental data sufficiently; however, the BVM model showed a better fit for calculating the measured current density outputs compared to the NM model. Using the mean values for the parameter distribution obtained from Monte Carlo-based simulations, the BVM model demonstrated an R^2 of 0.996 for the sweep down and an R^2 of 0.994 for the simulated data of the sweep up. The fitted values for the parameters I_{max}, α, E_{SP}, K_1, and K_2 are summarized in Table 1. The mean values of the simulated maximum current densities were 1370.88 and 1394.34 mA m^{-2} for the sweep down and sweep up, respectively. Furthermore, the BVM model predicted a transfer coefficient α of 0.55 for both data sets. As standard potential E_{SP}, −0.241 and −0.264 V were obtained from parameter fitting of the sweeps. Values of 2.19 and 2.86 were calculated by the model for the constant K_1. For K_2, a higher value compared to K_1 was observed with 8.18 and 8.56 for the sweep up and the sweep down, respectively.

Compared to the mean values obtained from the Monte Carlo-based simulation (Table 1), the NM model demonstrated an R^2 of 0.983 for the sweep down and an R^2 of 0.973 for the sweep up. Values of 1298.04 and 1330.89 mA m^{-2} were obtained, respectively, for the sweep data sets, based on fitting of the maximum current density I_{max}. The fitting resulted in E_{KA} parameter values of −0.160 V and −0.177 V, respectively.

The experimental data relating to applied potential and corresponding current density were described using both model approaches. Both models yielded an acceptable fit with the experimental data at lower and higher applied potentials (Fig. 7). At an electron flux of 20 %, the BVM model showed an R^2 value of 0.947, whereas at 50 % electron flux, an R^2 value of 0.941 was obtained (Table 2).

The BVM model predicted a set of parameters for the change of the potential to 20 % electron flux (Table 2). The simulated maximum current density was at 1169.04 mA m^{-2} and showed a transfer coefficient α value of 0.55. A theoretical standard potential −0.3 V and a substrate affinity constant K_M of 0.11 mmol L^{-1} were obtained from the parameter fitting. The K_1 value was significantly higher at 6.6 when compared to the constant K_2, which had a value of 1.04×10^{-7}. However, when the potential was changed to 50 % electron flux, the data set fit showed a maximum current density of 1083.39 mA m^{-2} with a transfer coefficient α of 0.45. A predicted value of −0.22 V was determined for the redox potential of acetate, and a substrate affinity constant K_M of 0.09 mmol L^{-1} was obtained. The simulation showed 6.53×10^{-6} for K_1 and 1.6 for K_2.

The NM model could describe the current densities in dependency of potential changes (Table 2). The simulation runs yielded values for I_{max}, E_{KA}, and K_S. The maximum current density obtained from the data set was 1160.83 mA m^{-2} for a potential change to 20 % electron flux and 1083.25 mA m^{-2} for 50 % electron flux. For the parameter E_{KA}, the simulation showed values of −0.197 V and −0.195 V, respectively. For the substrate affinity constant K_S, the calculation resulted in 0.08 and 0.09 mmol L^{-1} for a change in the potential to 20 % and 50 % electron flux.

The resulting simulation values were used to predict the current density outputs for possible changes in applied potentials concerning the electron flux. For instance, the current density at an electron flux of 35 % was calculated (Fig. 8). The predicted current output was compared to the experimental output in addition to the simulated data of the measured current densities during the 20 % and 50 % electron fluxes. The simulation was performed with the BVM model, and the parameters used were computed from the average of the adjusted parameters of 20 % and 50 % electron fluxes using 0.189 V and 0.2 V, respectively, as applied potentials.

4. Discussion

4.1. Robustness of RDBER

The stability of current output in addition to the robustness under varying conditions in a BES are key factors that could limit the application of this technology in an industrial context. This study analyzed the robustness in terms of current density of a 10 L RDBER for about 1.5 months of operations while the influence of various process variables on the performance of this system was monitored. Changes in applied potentials were chosen to simulate different electron fluxes in the system and were intentionally set to lower percentages. While the decrease in applied potential had immediate effect (as expected) on the current output in the system in relation to the linear sweep voltammetry, no

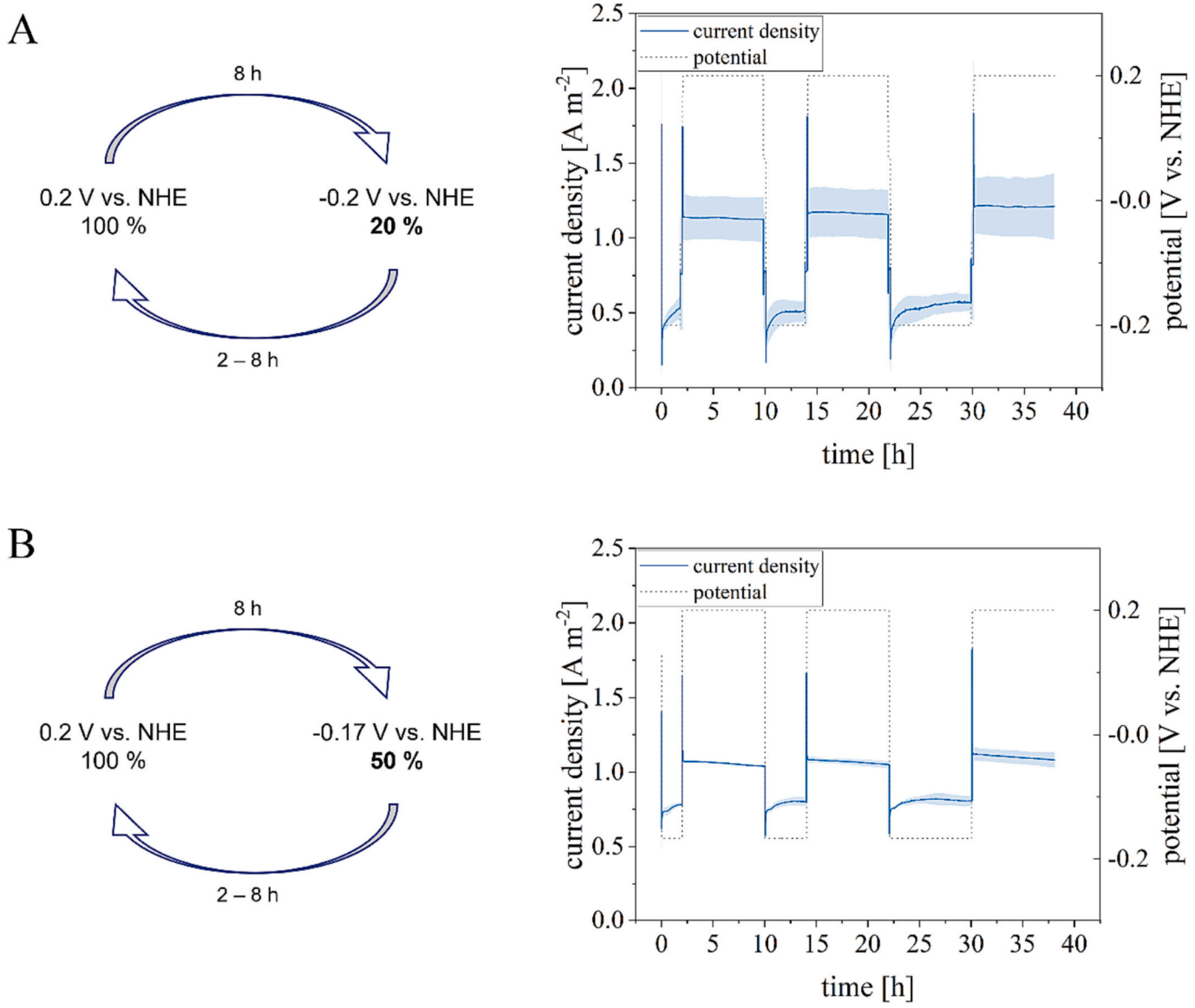

Fig. 4. Influence of potential alterations on performance. Electron flux (EF) was defined as a factor for produced current density. With this, 0 A m^{-2} was determined as 0 % EF, while the stable current of 1.2 A m^{-2} was defined as 100 % EF. Derived from this, 20 % and 50 % EF were chosen and the applied potentials of −0.2 V and −0.17 V, respectively, were obtained from the linear sweep voltammetry (Fig. 3) in which current density and therefore EF could be correlated to potential. Chosen potentials for 20 % EF (A) and 50 % EF (B) were applied for 2, 4, or 8 h, and altered with 8 h of a 100 % EF interval with a potential of 0.2 V. This regime of changing the potential was applied in triplicate alterations as indicated by the standard deviation shown in light blue. (For interpretation of the references to colour in this figure legend, the reader is referred to the web version of this article.)

lasting impact on the overall performance was found. The electron flux could be manipulated by the applied potential without any overall losses in system productivity. Manipulating the current density in accordance with the applied potential and the stability of the model biofilm has previously been reported in terms of slow continuous changes of anode potential within a batch laboratory scale system (Prokhorova et al., 2017). However, in this study, even the sudden drop in potential for time periods of 2 to 8 h was found to have no negative impact on current output. This stability would enable the long-term operation of a MEC with this defined mixed-species biofilm under varying power supply conditions without negatively impacting overall productivity. Accordingly, the fluctuations in the energy supply that could be expected in industrial applications might be rather unproblematic due to biofilm robustness.

Changes in rotational speed resulted in an expected decline while the discs spun more slowly, whereas an increased current was produced at a higher rotational speed. The design of the RDBER was derived from rotating biological contactors, in which the crossflow was adjusted by the rotational speed of the rotating biofilm substratum (Hassard et al., 2015). Thereby, different shear forces were applied to the anodic biofilm. The influence that different shear forces can have on bacterial biofilms was previously reported (Stoodley et al., 2002). Especially, in this system offering an active substratum, the shear force will have an impact on biofilm activity as it might shear off inactive cells, cause compactness of the biofilm, and thereby leading to an increase in biofilm conductivity or an increase in diffusive mass transfer from the bulk phase toward the anode. Especially in terms of anodic systems, it was reported that the limitation of biological activity is mainly due to a proton gradient from bulk phase to anode surface. This pH gradient might be flattened by an increase in availability of buffer from the medium.

Both process variables were chosen to simulate real process conditions that can be expected during industrial application of the RDBER. While short-term manipulation of substrate crossflow and electron

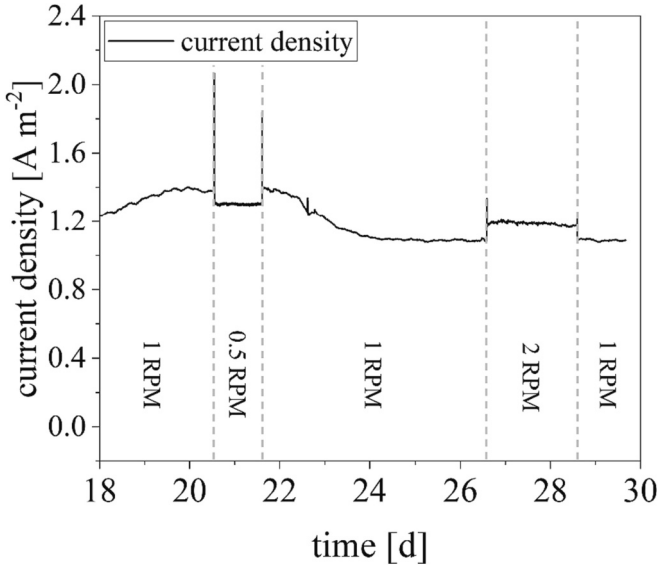

Fig. 5. Current density influenced by changes in rotational speed of the disc electrodes. Alternations in rotational speed were analyzed from days 18 to 30. Rotational speed was decreased from 1 to 0.5 RPM for 1 day followed by an interval of around four days of 1 RPM before the speed was increased to 2 RPM for 2 days. A decline in current density to 1.3 A m^{-2} was monitored at 0.5 RPM, while a slow decrease in the interval of 1 RPM for four days to a stable current density of 1.1 A m^{-2} could be measured. Increasing the rotational speed to 2 RPM led to an increase in this stable value to 1.2 A m^{-2}, which decreased again to the initial value of 1.1 A m^{-2} as soon as 1 RPM was applied again.

transfer rates were observed during the changes in rotational speed and applied potential, respectively, the long-term stability, robustness and steerability of the model biofilm was successfully demonstrated in this study as well. In addition, a CE of 113.3 % over 1.5 months of operation was achieved. CE values above 100 % indicate that additional electron donors were utilized for the conversion to electricity or H_2 in MFCs or MECs. *G. sulfurreducens* is known to use H_2 instead of acetate as an electron donor (Caccavo et al., 1994; Mollaei et al., 2021). As the RDBER was intentionally designed as a membrane-free system, H_2 shuttling from the cathode to the anode-reducing biofilm could have resulted in this high CE. Thereby, the modification that involves placing the cathode half-discs in the upper part of the RDBER as done in this study might have already caused a positive decrease in this H_2 shuttling in comparison to the design as described by Hackbarth et al. (2023). Further modifications might lead to even more improvements in the productivity of the system.

In the here studied RDBER, a stable current density of 1.2 ± 0.2 A m^{-2} over 1.5 months and a maximum current density of 1.8 A m^{-2} were achieved. In comparison, the study by Hackbarth et al. (2023) reported a maximum current density of 1.2 A m^{-2} and a stable current density of 0.9 A m^{-2} in a batch process over nine days with a mixed-species biofilm formed by *S. oneidensis* and *G. sulfurreducens*. The different cathode placement might have led to an improvement in the overall performance of the RDBER and, more importantly, this study provided insight into the long-term stability of the mixed-species biofilm over 1.5 months of operations.

4.2. Predictability and automatic steering of RDBER

In the next step, a mathematical process model based on the BVM and NM equations was applied (Hamelers et al., 2011). This model is an important step toward an automated system that controls BES process conditions based on stability and product formation of the overall process. This model is capable of predicting the current production based on the changes in applied potential. Hence, it is possible to direct the current density output of the reactor during steady state operations. Microbial electrolysis cells are used for the production of hydrogen and the

Table 1
Parameters from fitting the linear sweep voltammetry (LSV) data to the Butler–Volmer–Monod and Nernst–Monod (BVM and NM, respectively) models. I_{max} is the maximum current density, α the transfer coefficient, $E_{S/P}$ is the redox potential of acetate, and E_{KA} is the potential at half maximum current density. K_1 describes the rate of the biochemical reaction compared to the electrochemical reaction, and K_2 describes the ratio of the forward compared to the backward reaction of the redox component.

Fit	I_{max} [mA m^{-2}]	α	E_{SP}/E_{KA} [V]	K_1	K_2	R^2
BVM						
Sweep down	1370.88	0.55	−0.241	2.19	8.18	0.996
Sweep up	1394.34	0.55	−0.264	2.86	8.56	0.994
NM						
Sweep down	1298.04	–	−0.160	–	–	0.983
Sweep up	1330.89	–	−0.177	–	–	0.973

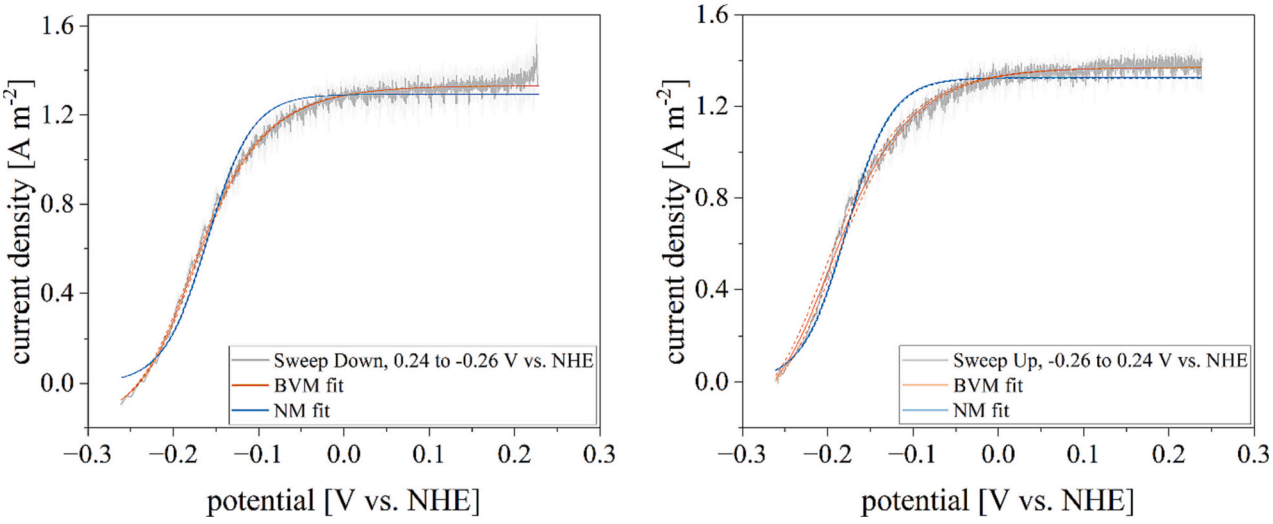

Fig. 6. Comparison of the model fits for Butler–Volmer–Monod and Nernst–Monod models (BVM and NM, respectively) to describe the linear sweep data sets. The dashed lines represent the 10 % and 90 % quantiles of the simulations. (For interpretation of the references to colour in this figure legend, the reader is referred to the web version of this article.)

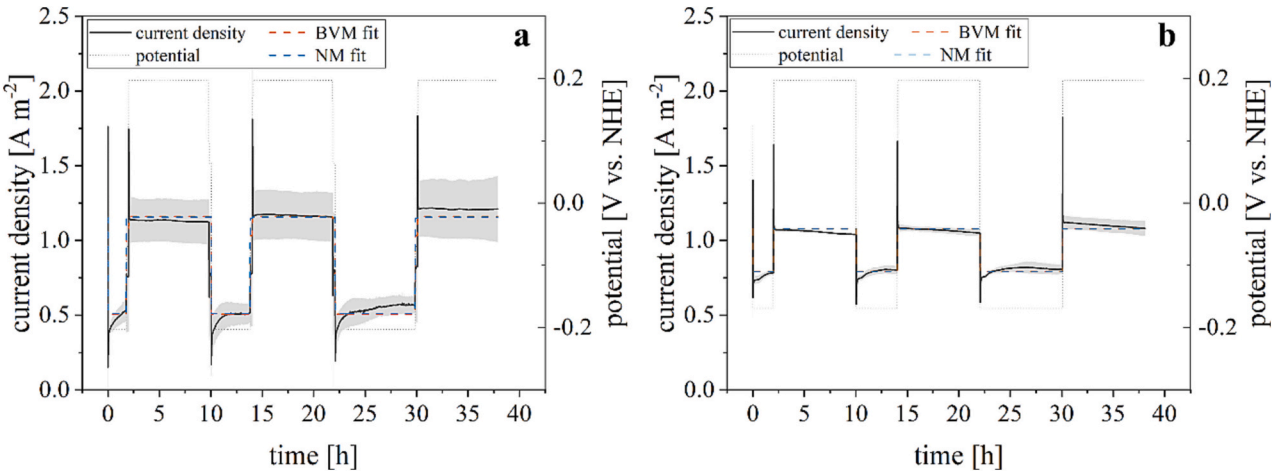

Fig. 7. Modeling of the changes in current density at different applied potentials referring to 20 % (a) and 50 % (b) of the maximum electron flux based on the BVM and NM models. (For interpretation of the references to colour in this figure legend, the reader is referred to the web version of this article.)

Table 2
Parameters from fitting the experimental data at 20 % and 50 % electron flux based on the BVM and NM models. I_{max} is the maximum current density, α the transfer coefficient, $E_{S/P}$ is the redox potential of acetate, E_{KA} is the potential at half maximum current density, K_1 describes the rate of the biochemical reaction compared to the electrochemical reaction, K_2 describes the ratio of the forward compared to the backward reaction of the redox component, K_M and K_S describe the substrate affinity.

Fit	I_{max} [mA/m^2]	α	E_{SP}/E_{KA} [V]	K_1	K_2	K_M/K_S [mmol L^{-1}]	R^2
BVM							
20 %	1169.04	0.55	−0.3	6.6	1.04×10^{-7}	0.11	0.947
50 %	1083.39	0.45	−0.22	6.53×10^{-6}	1.6	0.09	0.941
NM							
20 %	1160.83	–	−0.197	–	–	0.08	0.934
50 %	1083.25	–	−0.195	–	–	0.09	0.941

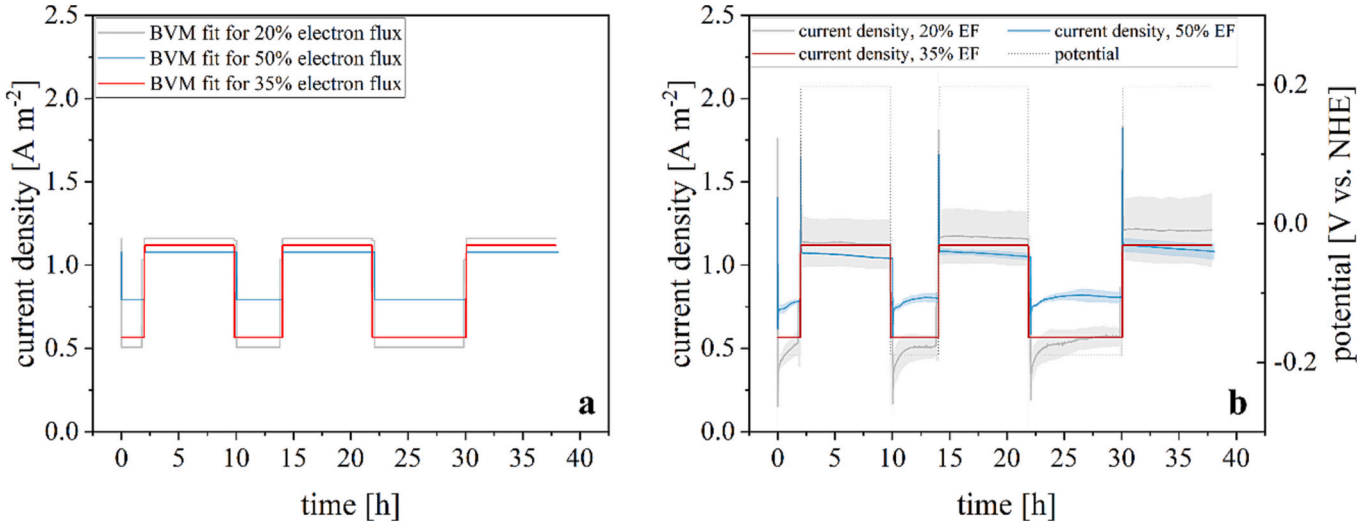

Fig. 8. Prediction of current density at 35 % electron flux (EF) using the BVM model compared to simulated data (a) and experimental data (b) for a potential change of 20 % and 50 % electron flux. (For interpretation of the references to colour in this figure legend, the reader is referred to the web version of this article.)

necessary energy input to the system will depend mostly on the anode potential. Therefore, by applying this model, it will be possible to dynamically react to changes in energy availability and price. The authors assume that the rapid response time and robustness of microbial electrolysis systems, such as the one presented in this study, are an advantage compared to typical large scale chemical processes that are not as flexible.

The BVM model is capable of more accurate descriptions of the polarization curves than the NM model as already shown by Hamelers et al. (2011). Compared to the NM equation, the BVM equation incorporates more parameters that describe additional bioelectrochemical subprocesses, which might be a possible reason for its enhanced fitting accuracy. The parameters obtained from fitting the linear sweep data set are in good agreement with the literature (Hamelers et al., 2011). The parameter K_1 indicates the ratio of the bioelectrochemical reaction to the electrochemical reaction (Hamelers

et al., 2011), which is very low for the fit at 50 % electron flux. A low value of K_1 that approaches zero leads to a BVM fit that approximates the shape of the NM model and the transfer coefficient would have a minor impact on the simulation. This impact can be observed by comparing the parameters K_1 and α between the BVM fitting of 20 % and 50 % electron fluxes. At 50 % electron flux, both parameters are low, and the calculation term of K_1 would tend toward zero. K_2 describes the ratio of the forward to backward reactions of the redox component and is expected to have numbers >1 because microorganisms utilize the substrate (Hamelers et al., 2011). However, this condition is not the case for the 20 % electron flux fit and the rate constant K_2 could cause larger fits within the same data set for K_1 and E_{SP}. Moreover, the simulated values for E_{SP} are in range with the reported redox potential of the electron donor acetate around −0.29 V (Thauer et al., 1977; Hamelers et al., 2010). The BVM model formulates the substrate affinity term, K_M, as a potential dependent, which differs from the NM model. Therefore, various K_M values are expected at different applied potentials in the BVM model. To simplify the parameter fitting and simulation runs, a fit was computed for the complete data set at 20 % and 50 % electron flux that resulted in a defined set of parameters for each condition. These values could be used in further simulations to predict current density outputs at various applied potentials. In addition, a constant substrate concentration of 20 mM was used since no substrate limitation was assumed during potential changes and steady-state conditions. At rather low values of K_S and high substrate concentrations, the Monod term of the NM equation tends toward a value of 1 and would have minimal or no effect on the current calculation. The E_{KA} value, which is defined as the potential at half the maximum current density, was discovered to be at −0.155 V for anode respiring bacteria (Torres et al., 2008), and the resulting parameters using the NM model for the various data sets are in the range with this literature value. In the future, this model could be extended to describe the limitations of nutrients in addition to the molecular diffusion of these nutrients into the biofilm during RDBER operation to facilitate long-term applications of this system.

5. Conclusion

In this study, a defined mixed-species anodic biofilm was characterized in terms of its stability regarding changes in applied anode potential and different applied shear forces. The robustness and long-term stability of this model biofilm were successfully demonstrated. Although the biofilm was exposed to rapid alternations in environmental conditions, a stable current production of 1.2 A m^{-2} could be monitored during 46 days of operations. Furthermore, a mathematical model was applied that was suitable to describe and even predict the current output as an effect of potential changes in the system. The BVM model showed better curve fitting than the NM model to describe polarization curves. In terms of fitting the data of potential changes, both model approaches appear to be suitable for calculations, and the simulation results are comparable with experimental data. With this setup, automatic control of the entire process could potentially be developed in the future, allowing long-term operations of this bioelectrochemical reactor for industrial applications.

CRediT authorship contribution statement

Melanie T. Knoll: Conceptualization, Data curation, Formal analysis, Investigation, Methodology, Software, Validation, Visualization, Writing – original draft, Writing – review & editing. **Nikolai Jürgensen:** Conceptualization, Data curation, Formal analysis, Investigation, Methodology, Software, Validation, Visualization, Writing – original draft, Writing – review & editing. **Janek R. Weiler:** Conceptualization, Data curation, Formal analysis, Investigation, Methodology, Software, Validation, Visualization. **Johannes Gescher:** Conceptualization, Funding acquisition, Project administration, Resources, Supervision, Writing – review & editing.

Declaration of competing interest

The authors declare that they have no known competing financial interests or personal relationships that could have appeared to influence the work reported in this paper.

Data availability

The data sets generated and analyzed during this study are shown in the manuscript or can be obtained from the corresponding author on reasonable request.

Acknowledgement

This work was financially supported from the project “Bio-electrochemical System for Flexible Biogas Production” of Fachagentur Nachwachsende Rohstoffe (grant number 2219NR051).

Appendix A. Supplementary data

Supplementary data to this article can be found online at https://doi.org/10.1016/j.biteb.2023.101640.

References

Arndt, L., Wiegmann, V., Kuchemüller, K.B., Baganz, F., Pörtner, R., Möller, J., 2021. Model-based workflow for scale-up of process strategies developed in miniaturized bioreactor systems. Biotechnol. Prog. 37, e3122.

Caccavo, F., Lonergan, D.J., Lovley, D.R., Davis, M., Stolz, J.F., McInerney, M.J., 1994. *Geobacter sulfurreducens* sp. nov., a hydrogen- and acetate-oxidizing dissimilatory metal-reducing microorganism. Appl. Environ. Microbiol. 60, 3752–3759.

Cerrillo, M., Viñas, M., Bonmatí, A., 2016. Overcoming organic and nitrogen overload in thermophilic anaerobic digestion of pig slurry by coupling a microbial electrolysis cell. Bioresour. Technol. 216, 362–372.

Chaudhuri, S.K., Lovley, D.R., 2003. Electricity generation by direct oxidation of glucose in mediatorless microbial fuel cells. Nat. Biotechnol. 21, 1229–1232.

Coppi, M.V., Leang, C., Sandler, S.J., Lovley, D.R., 2001. Development of a genetic system for *Geobacter sulfurreducens*. Appl. Environ. Microbiol. 67, 3180–3187.

Dolch, K., Danzer, J., Kabbeck, T., Bierer, B., Erben, J., Förster, A.H., Maisch, J., Nick, P., Kerzenmacher, S., Gescher, J., 2014. Characterization of microbial current production as a function of microbe-electrode-interaction. Bioresour. Technol. 157, 284–292.

Engel, C., Schattenberg, F., Dohnt, K., Schröder, U., Müller, S., Krull, R., 2019. Long-term behavior of defined mixed cultures of *Geobacter sulfurreducens* and *Shewanella oneidensis* in bioelectrochemical systems. Front. Bioeng. Biotechnol. 7, 60.

Hackbarth, M., Gescher, J., Horn, H., Reiner, J.E., 2023. A scalable, rotating disc bioelectrochemical reactor (RDBER) suitable for the cultivation of both cathodic and anodic biofilms. Bioresour. Technol. Rep. 21, 101357.

Hamelers, H.V.M., Heijne, A. ter, Sleutels, Tom H.J.A., Jeremiasse, A.W., Strik, David P. B.T.B., Buisman, C.J.N., 2010. New applications and performance of bioelectrochemical systems. Appl. Microbiol. Biotechnol. 85, 1673–1685.

Hamelers, H.V.M., Heijne, A. ter, Stein, N., Rozendal, R.A., Buisman, C.J.N., 2011. Butler-Volmer-Monod model for describing bio-anode polarization curves. Bioresour. Technol. 102, 381–387.

Hassanein, A., Witarsa, F., Guo, X., Yong, L., Lansing, S., Qiu, L., 2017. Next generation digestion: complementing anaerobic digestion (AD) with a novel microbial electrolysis cell (MEC) design. Int. J. Hydrog. Energy 42, 28681–28689.

Hassard, F., Biddle, J., Cartmell, E., Jefferson, B., Tyrrel, S., Stephenson, T., 2015. Rotating biological contactors for wastewater treatment – a review. Process. Saf. Environ. Prot. 94, 285–306.

Kadier, A., Simayi, Y., Abdeshahian, P., Azman, N.F., Chandrasekhar, K., Kalil, M.S., 2016. A comprehensive review of microbial electrolysis cells (MEC) reactor designs and configurations for sustainable hydrogen gas production. Alex. Eng. J. 55, 427–443.

Knoll, M.T., Fuderer, E., Gescher, J., 2022. Sprayable biofilm - agarose hydrogels as 3D matrix for enhanced productivity in bioelectrochemical systems. Biofilm. 4, 100077.

Logan, B.E., 2009. Exoelectrogenic bacteria that power microbial fuel cells. Nat. Rev. Microbiol. 7, 375–381.

Maurya, R., Das, R., Tripathi, A.K.Neergat, 2022. Relationship between the electron-transfer coefficients of the oxygen reduction reaction estimated from the Gibbs free energy of activation and the Butler-Volmer equation. Phys. Chem. Chem. Phys. 25, 700–707.

Möhle, R.B., Langemann, T., Haesner, M., Augustin, W., Scholl, S., Neu, T.R., Hempel, D. C., Horn, H., 2007. Structure and shear strength of microbial biofilms as determined with confocal laser scanning microscopy and fluid dynamic gauging using a novel rotating disc biofilm reactor. Biotechnol. Bioeng. 98, 747–755.

Mollaei, M., Timmers, P.H.A., Suarez-Diez, M., Boeren, S., van Gelder, A.H., Stams, A.J. M., Plugge, C.M., 2021. Comparative proteomics of *Geobacter sulfurreducens* PCAT in

response to acetate, formate and/or hydrogen as electron donor. Environ. Microbiol. 23, 299–315.
Moser, A., Kuchemüller, K.B., Deppe, S., Hernández Rodríguez, T., Frahm, B., Pörtner, R., Hass, V.C., Möller, J., 2021. Model-assisted DoE software: optimization of growth and biocatalysis in *Saccharomyces cerevisiae* bioprocesses. Bioprocess Biosyst. Eng. 44, 683–700.
Prokhorova, A., Sturm-Richter, K., Doetsch, A., Gescher, J., 2017. Resilience, dynamics, and interactions within a model multispecies exoelectrogenic-biofilm community. Appl. Environ. Microbiol. 83, e03033-16.
Recio-Garrido, D., Perrier, M., Tartakovsky, B., 2016. Modeling, optimization and control of bioelectrochemical systems. Chem. Eng. J. 289, 180–190.
Stoodley, P., Cargo, R., Rupp, C.J., Wilson, S., Klapper, I., 2002. Biofilm material properties as related to shear-induced deformation and detachment phenomena. J. Ind. Microbiol. Biotechnol. 29, 361–367.
Thauer, R.K., Jungermann, K., Decker, K., 1977. Energy conservation in chemotrophic anaerobic bacteria. Bacteriol. Rev. 41, 100–180.
Torres, C.I., Marcus, A.K., Rittmann, B.E., 2007. Kinetics of consumption of fermentation products by anode-respiring bacteria. Appl. Microbiol. Biotechnol. 77, 689–697.
Torres, C.I., Marcus, A.K., Parameswaran, P., Rittmann, B.E., 2008. Kinetic experiments for evaluating the Nernst-Monod model for anode-respiring bacteria (ARB) in a biofilm anode. Environ. Sci. Technol. 42, 6593–6597.
Venkateswaran, K., Moser, D.P., Dollhopf, M.E., Lies, D.P., Saffarini, D.A., MacGregor, B. J., Ringelberg, D.B., White, D.C., Nishijima, M., Sano, H., Burghardt, J., Stackebrandt, E., Nealson, K.H., 1999. Polyphasic taxonomy of the genus *Shewanella* and description of *Shewanella oneidensis* sp. nov. Int. J. Syst. Bacteriol. 49, 705–724.
Yin, Q., Zhu, X., Zhan, G., Bo, T., Yang, Y., Tao, Y., He, X., Li, D., Yan, Z., 2016. Enhanced methane production in an anaerobic digestion and microbial electrolysis cell coupled system with co-cultivation of *Geobacter* and *Methanosarcina*. J. Environ. Sci. 42, 210–214.